Elastic anisotropy and incohesive bond of chemical-vapor-deposition diamond film: Acoustic resonance measurements and micromechanics modeling

Nobutomo Nakamura,[a] Hirotsugu Ogi, Tetsu Ichitsubo, and Masahiko Hirao
Graduate School of Engineering Science, Osaka University, Machikaneyama 1-3, Toyonaka, Osaka 560-8531, Japan

Natsuo Tatsumi, Takahiro Imai, and Hideaki Nakahata
Itami R & D Laboratories, Sumitomo Electric Industries, Ltd., Itami, Hyogo 664-0016, Japan

(Received 3 February 2003; accepted 27 August 2003)

This article studies elastic anisotropy of chemical vapor deposition (CVD) polycrystalline diamond films using acoustic spectroscopy and micromechanics modeling. CVD diamond films often exhibit elastic anisotropy between the film-growth direction and in-plane direction and show five independent elastic constants. They are denoted by C_{11}, C_{33}, C_{13}, C_{44}, and C_{66} when the x_3 axis lies along the film-growth direction. Measurements of thickness resonance frequencies and free-vibration resonance frequencies of the diamond film deduce four independent elastic constants among them, including C_{44} and C_{66}, with which the elastic anisotropy is discussed. The anisotropy between the shear moduli is 5%–10%. The elastic constants are remarkably smaller than those of an isotropic polycrystalline diamond. We attribute the anisotropy and small elastic constants of the CVD diamond film to local incomplete cohesion. This view is supported by a micromechanics calculation. © *2003 American Institute of Physics.* [DOI: 10.1063/1.1620376]

I. INTRODUCTION

Diamond films have received intensive study by many researchers,[1–6] because they can improve many crystal-system devices with their outstanding stiffness, thermal conductivity, electric insulativity, and optical refractivity. The largest elastic-stiffness coefficients, for example, meet the need for a gigahertz-frequency surface acoustic wave (SAW) device.[6] Recent advancement of the chemical vapor deposition (CVD) technique makes those applications possible.

Elastic-stiffness coefficients C_{ij} are indispensable to designing such an application as a SAW filter. They also reflect the material's bond strength, which is difficult to evaluate with conventional methods as scanning electron microscopy (SEM) and transmission electron microscopy (TEM). Thus, measurement of a diamond-film C_{ij} remains an important issue. Several studies reported diamond-film elastic constants, assuming it to be elastically isotropic.[1,2] However, a polycrystalline diamond thin film macroscopically shows elastic anisotropy between the directions parallel and normal to the film surface. This occurs because of the columnar structure, texture, residual stress, and local incohesive bonds (or microcracks). Thus, a diamond thin film will show transverse isotropy (or hexagonal symmetry) with five independent elastic-stiffness coefficients. They are denoted by C_{11}, C_{33}, C_{13}, C_{44}, and C_{66} with a coordinate system, where the x_3 axis is along the film-growth direction, and the x_1 and x_2 axes lie parallel to the film surface. Most previous studies on film's elastic constants reported only the in-plane Young's modulus E_1 using the static bending test[3] and flexural vibration of a reed composed of a film/substrate layered plate.[7] These methods always involve ambiguity caused by the mechanical contact needed for gripping the specimen and for the acoustic transduction. The Brillouin-scattering technique[4,8] provides a noncontacting method, but it failed to detect the elastic anisotropy because it is insensitive to non Rayleigh-wave acoustic modes and the resulting C_{ij} includes uncertainty, typically more than 10%. Thus, no study has reported the elastic anisotropy on a CVD diamond film.

Here, we determine the C_{ij} of diamond films deposited by the CVD technique using two acoustic-resonance-spectroscopic methods: (i) electromagnetic acoustic resonance (EMAR)[9] and (ii) resonance ultrasound spectroscopy (RUS).[10–13] The EMAR method measures the thickness resonance frequencies of a longitudinal-plane wave and a polarized shear-plane wave propagating in the film-growth direction. These frequencies are closely related to the C_{33} and C_{44}, respectively. The RUS method measures the free-vibration resonance frequencies of the specimen to deduce the remaining three elastic constants. Combination of the two resonance methods determines all the elastic constants of the film in principle. (However, the C_{33} was unavailable in the present study because of the upper limit of frequency range of the instrument we used.)

We find 5%–10% anisotropies in the shear moduli between the in-plate and the film-growth directions. We attribute this anisotropy to a local incohesive bond, and confirm this view by developing micromechanics modeling.

II. MATERIAL

The diamond films were deposited on a (001) surface of a monocrystal silicon substrate by the microwave-plasma

[a]Author to whom correspondence should be addressed; electronic mail: nobutomo@me.es.osaka-u.ac.jp

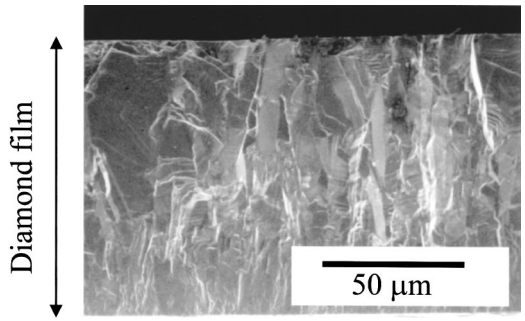

FIG. 1. SEM image of the cross-section of diamond film deposited by the microwave-plasma CVD method.

CVD technique reported elsewhere.[5] The film surface was mechanically polished to obtain a flat surface and then the silicon substrate was chemically removed. Figure 1 shows the microstructure of cross section of the CVD diamond: a columnar structure is observed. Two specimens were machined: (i) 0.525-mm-thick rectangular parallelepiped CVD diamond with $5.012\times5.003\ \mathrm{mm}^2$ faces, and (ii) 0.289-mm-thick disk-shape CVD diamond with 20.012 mm diameter. We also used (iii) a rectangular-parallelepiped-shape high-purity monocrystal diamond, measuring $4.026\times4.025\times0.478\ \mathrm{mm}^3$ for comparison. This was fabricated by the ultrahigh pressure synthetic method.

X-ray diffraction spectrum of the CVD diamond specimens showed large (220) peaks as seen in Fig. 2, indicating that the (110) crystallographic planes are preferentially oriented parallel to the film surface. This is in agreement with Djemia's result on a CVD diamond film.[4] The lattice parameter deduced from the x-ray measurements was 3.567 ± 0.001 Å for each specimen, which is identical to that of a monocrystal diamond.[14]

III. MEASUREMENT METHODS

A. Thickness resonance and EMAR

An electromagnetic acoustic transducer (EMAT)[9] can excite and detect ultrasound vibration in electrically conductive materials without any contact through the Lorentz-force mechanism and/or the magnetostriction effect. EMATs usually show a low efficiency of conversion between the electromagnetic fields and elastic waves. However, by superimposing reflection echoes coherently in a resonance state, the efficiency remarkably increases. This method is called

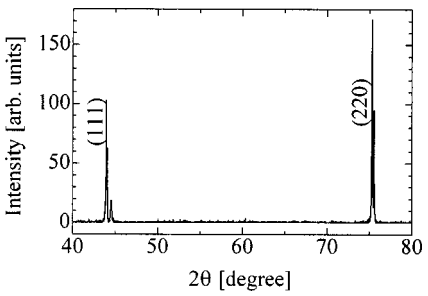

FIG. 2. X-ray-diffraction spectrum on the x_3 face of the 0.289-mm-thick CVD polycrystalline diamond specimen.

EMAR. EMAR makes it possible to measure the thickness resonance frequencies of the longitudinal and shear waves propagating in the film-growth direction with a high accuracy.[15] We used a bulk-wave EMAT.[9] It consists of a spiral-elongated coil and a pair of permanent magnets mounted to the coil to simultaneously generate and detect a longitudinal wave and a shear wave polarized parallel to the film surface through the Lorentz-force mechanism. The same EMAT receives the reflected and overlapped echo signals. A frequency scan provides the resonance spectrum and the Lorentzian function fitting determines the resonance frequencies. The resonance frequencies of the longitudinal and shear ultrasounds depend on the film C_{33} and C_{44}, respectively, as well as the thickness and mass density. The films C_{33} and C_{44} are determined by measuring the resonance frequencies.

Because diamond is nonconductive, we deposited a 300-nm-thick Au film on a specimen's surface so as to make the Lorentz-force coupling possible. The deposition should change the resonance frequencies. Although the frequency shifts are estimated to be 1% at most, we eliminated this effect using the frequency equation for a double-layered plate, which was derived by considering four partial plane waves traveling along the x_3 direction. The resulting expression takes the form[15]

$$C_{\mathrm{Au}}k_{\mathrm{Au}}\tan k_{\mathrm{Au}}d_{\mathrm{Au}}=C_{\mathrm{dia}}k_{\mathrm{dia}}\tan k_{\mathrm{dia}}d_{\mathrm{dia}}. \tag{1}$$

Here, C_i, d_i, k_i ($i=$ diamond or Au) are the elastic constants either of the longitudinal mode (C_{33}) or shear mode (C_{44}), thickness, and wave number $k=2\pi f/v$ with wave velocity v and resonance frequency f. Equation (1) yields C_{33} or C_{44} of the diamond film with the measured resonance frequencies and other known quantities.

B. Free-vibration resonance and RUS

The remaining three elastic constants (C_{11}, C_{12}, and C_{13}) were determined by the RUS method.[10–13] Free-vibration resonance frequencies of a solid specimen depend on the dimensions, the mass density, and all the C_{ij} of the solid. Then, the film C_{ij} can be determined from the measured resonance frequencies of free vibrations by an inverse calculation. This procedure has been established by several researchers.[10–13]

Figure 3 shows the measurement setup. The specimen was put on the piezoelectric tripod consisting of two pinducers and one support. One pinducer generates a sinusoidal continuous-wave (cw) signal in the specimen and the other pinducer detects the amplitude of vibration. Sweeping the frequency of the cw signal for excitation and measuring the oscillation amplitude as a function of the frequency, the resonance spectrum is obtained, which consists of many resonance peaks. Fitting the Lorentzian function around these peaks determines the free-vibration resonance frequencies. Because the piezoelectric tripod requires no coupling agent between the transducers and specimen, and no external force except for specimen weight, an ideal free vibration results.

The conventional RUS method, however, has a serious problem. In determining the C_{ij} inversely from the measured resonance frequencies, one must compare between a mea-

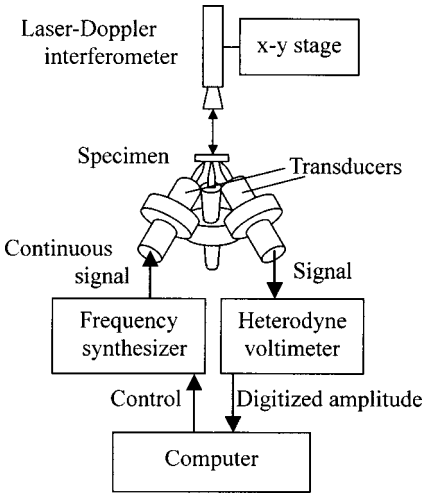

FIG. 3. Measurement setup of the RUS/laser technique.

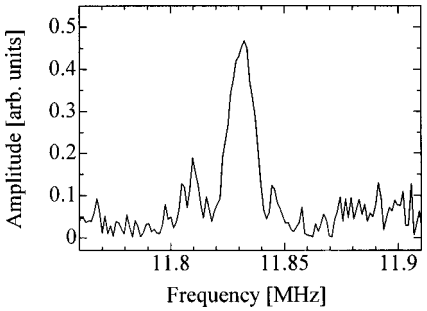

FIG. 4. Measured EMAR spectrum of the 0.525-mm-thick polycrystalline CVD diamond.

surement and a calculation referring to the same resonance mode (mode identification). Since many resonance peaks exist and they often overlap, it is quite difficult to identify them. If mode misidentification is included in the inverse calculation, the resultant C_{ij} has no physical meaning. In order to achieve the correct mode identification, we measured the out-of-plane displacement of the vibrating specimen at each resonance mode using laser-Doppler interferometry. By comparing the measured and computed displacement distributions, we achieved unambiguous mode identification, leading to the correct elastic constants. Since diamond is transparent, the Au-deposited surface was used for this measurement.

IV. RESULTS

Table I shows the monocrystal-diamond C_{ij} measured in the present study using the RUS method. They are consistent with reported values.[16] We calculated the C_{ij} of an isotropic polycrystalline diamond from the measured monocrystal C_{ij} using the Hill approximation.

Figure 4 shows the resonance spectrum of the thickness resonance of the shear wave for the 0.525-mm-thick CVD diamond. The C_{44} was calculated from the measured resonance frequency and C_{44} of Au ($=27.6$ GPa[17]) using Eq. (1). The resulting C_{44} were 532.6 ± 3.7 and 532.5 ± 3.7 GPa for the 0.289-mm-thick and 0.525-mm-thick specimens, respectively, being identical. The error bands arise from the resonance-frequency measurement errors; we measured the resonance frequencies ten times for each specimen and obtained the error bands. The C_{44} of the CVD diamond film agrees well with the shear modulus of the polycrystalline diamond. We could not determine the C_{33} because of the upper frequency limit (~22 MHz) of our instrument, beyond which the resonance frequencies of the longitudinal wave will occur.

Figure 5 shows an observed resonance spectrum measured by the RUS method. The resonance-peak heights varied depending on the positions of contacts between pinducers and specimen, but the resonance frequencies did not change. Figure 6 exemplifies the computed and measured displacement distributions of the vibrating specimen. The mode notation follows Mochizuki.[18] We see excellent agreement between the computed and measured distributions, which ensures the correct mode identification.

After an inverse calculation, we can calculate the sensitivity of each elastic constant to the resonance frequencies, that is, $\partial f/\partial C_{ij}$.[12] Using the sensitivity and errors in measured resonance frequencies (smaller than 10^{-4}), we estimated the accuracy of the resulting elastic constants. In Table I, we show the determined elastic constants and in-plate Young's modulus (E_1) calculated from the C_{ij}. Although E_1 depends on C_{33}, the contribution of C_{33} to E_1 is so small ($\partial E_1/\partial C_{33}<10^{-3}$) that we used the isotropic C_{33} in the calculation of E_1.

TABLE I. Elastic constants of monocrystal and polycrystalline diamonds (GPa).

	Monocrystal		Polycrystal						
				0.289 mm thick (hexagonal)					
	Present (cubic)	Reference 16 (cubic)	Aggregated (isotropic)	Measurement	Micromechanics	0.525 mm thick (hexagonal)	(110) texture (hexagonal)	(100) texture (hexagonal)	(111) texture (hexagonal)
C_{11}	1068.6 ± 2.1	1076.0	1143.0	1126.5 ± 0.1	1117.0	1070.3 ± 0.2	1150.4	1114.7	1163.2
C_{33}	1068.6 ± 2.1	1076.0	1143.0	—	1143.0	—	1162.9	1068.6	1197.4
C_{12}	119.8 ± 1.7	125.0	82.6	116.9 ± 1.4	79.4	106.5 ± 3.9	85.1	119.8	55.4
C_{13}	119.8 ± 1.7	125.0	82.6	139.3 ± 4.8	80.6	—	72.7	73.7	89.6
C_{44}	571.0 ± 0.3	575.8	530.2	532.6 ± 3.7	524.6	532.5 ± 0.5	520.5	571.0	504.7
C_{66}[a]	571.0 ± 0.3	575.8	530.2	504.8 ± 0.03	518.8	481.9 ± 0.04	532.6	520.5	536.8
E_1	1044.4 ± 4.5	1038.8	1131.8	1100.8 ± 0.04	1107.0	1024.6 ± 0.1	1140.2	1098.0	1154.1

[a]$C_{66}=(C_{11}-C_{12})/2$.

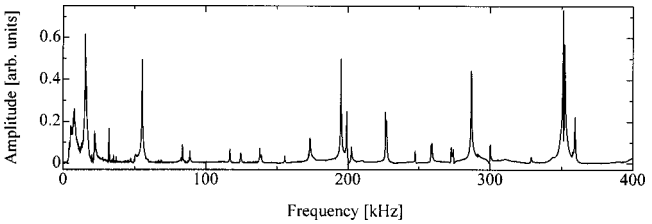

FIG. 5. Measured RUS spectrum of the 0.525-mm-thick polycrystalline CVD diamond.

There are two significant observations. First, C_{11}, E_1, and C_{66} of the CVD polycrystalline diamonds are smaller than those of the isotropic diamond. For the 0.289-mm-thick specimen, C_{11}, E_1, and C_{66} are smaller than those of the isotropic diamond by 1.5%, 3%, and 1.5%, respectively; and for the 0.525-mm-thick specimen, they are smaller by 6.5%, 11%, and 6%, respectively. Second, the C_{44} of the 0.289-mm-thick and 0.525-mm-thick CVD diamond films are larger than their C_{66} by 5.5% and 10.5%, respectively. This indicates that the CVD polycrystalline diamond is elastically anisotropic.

V. DISCUSSION

We consider following three possible causes for the above two observations; (i) residual stress, (ii) texture, and (iii) local incohesive regions. Residual stress changes the atomic distance and the elastic constants because of lattice anharmonicity. However, the lattice parameters of the CVD polycrystalline diamonds determined by the x-ray diffraction are identical to that of a monocrystal diamond, suggesting that the residual stress is small if any. The residual stress is usually caused by a mismatch of thermal expansion coefficients between the film and substrate. Because the substrate has been removed, the major part of the residual stress should be released. Thus, the residual stress cannot explain the observations.

Second, we consider the effect of texture. As seen in the x-ray-diffraction spectrum (Fig. 2), the film-growth direction (x_3) is oriented preferentially in the $\langle 110 \rangle$ directions. We calculated the macroscopic C_{ij} of such a textured microstructure that all the (110) planes of the columnar grains are aligned parallel to the x_3 surface with random rotation in-plane orientation around the x_3 axis. The Hill approximation was used for this calculation

$$\langle C_{ij} \rangle_{\text{Voigt}} = \frac{1}{2\pi} \int_0^{2\pi} C_{ij} d\theta,$$

$$\langle S_{ij} \rangle_{\text{Reuss}} = \frac{1}{2\pi} \int_0^{2\pi} S_{ij} d\theta, \tag{2}$$

$$\langle C_{ij} \rangle_{\text{Hill}} = \frac{\langle C_{ij} \rangle_{\text{Voigt}} + \langle S_{ij} \rangle_{\text{Reuss}}^{-1}}{2}.$$

Here, S_{ij} denote components of the elastic compliance matrix and θ is the rotational angle about the x_3 axis. Diamond exhibits a low anisotropic factor ($A = 1.2$), for which the Hill average method is known to provide good approximation for the aggregated C_{ij}. The calculated C_{ij} for the (110) texture are shown in Table I. [For comparison, the calculations for (111) and (100) textured films are also given.] The C_{66} is larger than C_{44} in the case of the (110) texture; this result is opposite to the observed results. Furthermore, the E_1 is larger than that of the isotropic case, being an opposite relationship to the observations again. Thus, the texture cannot be a dominant factor for the observations.

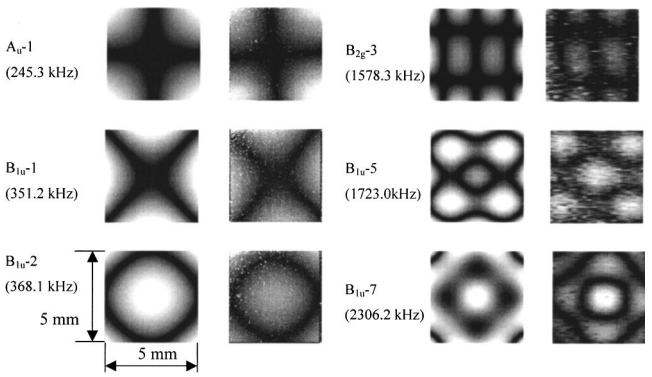

FIG. 6. Computed (left) and measured (right) surface displacements of the vibrating specimen. Mode notation follows Mochizuki (Ref. 18).

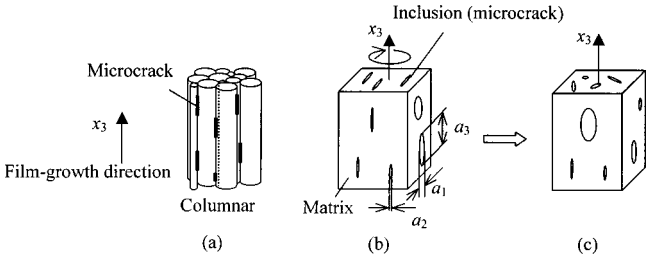

FIG. 7. Modeling of the CVD polycrystalline diamond with isotropic matrix and microcrack inclusions.

We finally consider the presence of many incohesive interfaces at the columnar grain boundaries. As seen in Fig. 1, CVD polycrystalline diamond consists of the columnar structure. It is known that microcracks, graphite, and amorphous carbon could occur on the boundaries of the columnar grains during the CVD process, causing such incohesive-bond regions. They will be negligible in the volume-fraction point of view, but their influence on the elastic properties can be remarkable, because the presence of such thin oriented weak-bond regions softens the material and causes elastic anisotropy. We investigate the effect by developing a micromechanics modeling. We assume the material to be a composite consisting of two phases: (i) isotropic matrix of polycrystalline diamond and (ii) thin ellipsoidal-shape microcracks aligned along the columnar grain boundaries (see Fig. 7).

The elastic constants $\mathbf{C}_C$ of a two-phase composite are calculated using Eshelby's equivalent inclusion theory[19] and Mori-Tanaka's mean field theory[20] as

$$\mathbf{C}_C = \mathbf{C}_M + [f_I(\mathbf{C}_I - \mathbf{C}_M)\mathbf{A}_d][f_M\mathbf{I} + f_I\mathbf{A}_d]^{-1},$$
$$\mathbf{A}_d = [\mathbf{S}\mathbf{C}_M^{-1}(\mathbf{C}_I - \mathbf{C}_M) + \mathbf{I}]^{-1}, \tag{3}$$

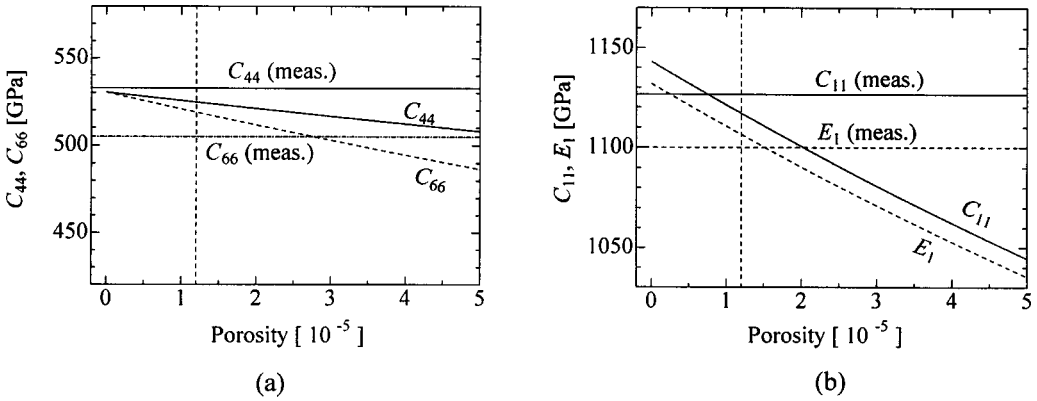

FIG. 8. Calculated elastic constants of the CVD diamonds with the micromechanics modeling: (a) C_{44} and C_{66} and (b) C_{11} and E_1. Measurements are for the 0.289-mm-thick film.

where $\mathbf{C}_M$ and $\mathbf{C}_I$ are elastic-constant tensors of the matrix and inclusions, respectively, and $\mathbf{S}$ is Eshelby's tensor. f_M and f_I are volume fractions of the matrix and inclusion. Eshelby's tensor depends on the shape of inclusion and Poisson's ratio of the isotropic matrix. When the inclusions are ellipsoids, the nonzero components of $\mathbf{S}$ become simple as tabulated in Mura's monograph.[21]

Figure 7 shows the procedure of analysis. Using Eq. (3), we determine the C_{ij} of a composite material that consists of the isotropic matrix and thin elliptical-shape inclusions ($a_3 > a_1 \gg a_2$), whose axes are aligned along the three principal coordinate axes [Fig. 7(b)]. This composite shows orthorhombic symmetry and has nine independent elastic constants. The elastic constants are then averaged around the x_3 axis using Eq. (2) [Fig. 7(c)]. Thus, we simulate the incohesive interfaces, distributed randomly along the columnar boundaries, keeping their major axes oriented along the film-growth direction.

We assumed zero modulus for the microcracks and $a_3:a_1:a_2=5:1:0.0005$. (The ratio of a_3/a_1 hardly affected the calculations.) Figure 8 shows the calculated C_{ij} as a function of the inclusion's volume fraction. All volume fraction provides C_{44} larger than C_{66}, which is consistent with the observations. When the porosity is near 1.2×10^{-5}, the calculation gives the diagonal components of the elastic constants and in-plane Young's modulus E_1 close to those of the 0.286-mm-thick specimen. For the 0.525-mm-thick specimen, the calculation provides the C_{ij} close to the measurements with the porosity of 4.0×10^{-5}. The 0.286 and 0.525 mm films have different porosities, which suggests a film-thickness dependence of porosity. This is no surprise because individual thin films are unique, depending on many factors such as pressure during deposition, concentration of source gas, temperature of substrate, residual stress, etc. For copper thin films a film-thickness dependence of volume fraction of defects is suggested.[22] The cause of the film-thickness dependence of porosity here has not been clarified, but our micromechanics model essentially explains both small elastic constants and elastic anisotropy of the CVD diamond films.

Calculations for the nondiagonal components (C_{13}, C_{12}) differ from the measurements. These elastic constants contribute little to the calculations and are therefore vulnerable to factors in the analysis (shape, aspect ratio, porosity, and so on). The exact properties of the inclusion are required to predict them correctly.

VI. CONCLUSIONS

In this study, a combination of the EMAR and RUS method determined the independent elastic constants of CVD diamond films including C_{44}, which was unavailable with conventional methods. The elastic constants of the CVD diamond film are smaller than those of the isotropic polycrystalline diamond and they show elastic anisotropy between the film-growth direction and the in-plate direction. The residual stress, texture, and incohesive grain boundaries in the columnar structure were considered to be the causes of these observations. We conclude that only the incohesive grain boundaries could explain the measurements. This was supported by micromechanics modeling. It is difficult to evaluate such incohesive boundaries with conventional SEM and TEM observations. Accurate ultrasonic measurement of the overall elastic constants of films provides information on the bond strength, which will be directly related to strength of the material.

To date, few researchers discussed the elastic anisotropy of the CVD diamond films on the basis of an accurate measurement of the elastic constants. The elastic anisotropy observed in this study will contribute to improvement of various acoustic devices.

[1] G. Lehmann, M. Schreck, L. Hou, J. Lambers, and P. Hess, Diamond Relat. Mater. **10**, 686 (2001).
[2] R. Kuschnereit, P. Hess, D. Albert, and W. Kulisch, Thin Solid Films **312**, 66 (1998).
[3] F. Szuecs, M. Werner, R. S. Sussmann, C. S. J. Pickles, and H. J. Fecht, J. Appl. Phys. **86**, 6010 (1999).
[4] P. Djemia, C. Dugautier, T. Chauveau, E. Dogheche, M. I. De Barrors, and L. Vandenbulcke, J. Appl. Phys. **90**, 3771 (2001).
[5] S. Kamiya, M. Sato, M. Saka, and H. Abe, J. Appl. Phys. **86**, 224 (1999).
[6] S. Shikata, H. Nakahata, A. Hachigo, and N. Fujimori, Diamond Relat. Mater. **2**, 1197 (1993).
[7] S. Sakai, H. Tanimoto, and H. Mizubayashi, Acta Mater. **47**, 211 (1999).
[8] A. L. Moretti, W. M. Robertson, B. Fisher, and R. Bray, Phys. Rev. B **31**, 3361 (1985).
[9] M. Hirao and H. Ogi, *EMATs for Science and Industry* (Kluwer, Boston, 2003).

[10] I. Ohno, J. Phys. Earth **24**, 355 (1976).
[11] H. Ledbetter, C. Fortunko, and P. Heyliger, J. Appl. Phys. **78**, 1542 (1995).
[12] A. Migliori, F. Sarrao, W. M. Visscher, T. M. Bell, M. Lei, Z. Fisk, and R. G. Leisure, Physica B **183**, 1 (1993).
[13] H. H. Demarest, Jr., J. Acoust. Soc. Am. **49**, 768 (1971).
[14] Natl. Bur. Stand. Circ. (U. S.) **539**, 25 (1953).
[15] H. Ogi, G. Shimoike, M. Hirao, K. Takashima, and Y. Higo, J. Appl. Phys. **91**, 4857 (2002).
[16] H. J. McSkimin and W. L. Bond, Phys. Rev. **105**, 116 (1957).
[17] R. F. S. Hearmon, Rev. Mod. Phys. **18**, 409 (1946).
[18] E. Mochizuki, J. Phys. Earth **35**, 159 (1987).
[19] J. D. Eshelby, Proc. R. Soc. London, Ser. A **241**, 376 (1957).
[20] T. Mori and K. Tanaka, Acta Metall. **21**, 571 (1973).
[21] T. Mura, *Micromechanics of Defects in Solids*, 2nd ed. (Martinus Nijhoff, The Hague, 1987), p. 394.
[22] R. Schwaiger, G. Dehm, and O. Kraft, Philos. Mag. A **83**, 693 (2003).